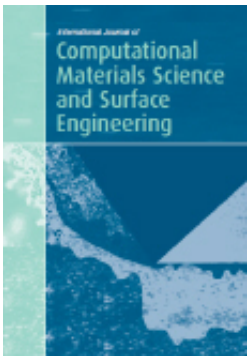

International Journal of Computational Materials Science and Surface Engineering

ISSN online: 1753-3473 - ISSN print: 1753-3465
https://www.inderscience.com/ijcmsse

Corrosion estimation of Cu and Br based automotive parts exposed to biodiesel environment: case of RSM and ANN

Olusegun David Samuel, Amin Taheri-Garavand, Marcus A. Amuche, Christopher C. Enweremadu

DOI: 10.1504/IJCMSSE.2023.10056070

Article History:

Received:	06 September 2022
Last revised:	07 September 2022
Accepted:	24 October 2022
Published online:	08 January 2024

Corrosion estimation of Cu and Br based automotive parts exposed to biodiesel environment: case of RSM and ANN

Olusegun David Samuel*

Department of Mechanical Engineering,
Federal University of Petroleum Resources,
Effurun, Delta State P.M.B 1221, Nigeria

and

Department of Mechanical Engineering,
University of South Africa,
Science Campus, Private Bag X6, Florida, 1709, South Africa
Email: samuel.david@fupre.edu.ng
*Corresponding author

Amin Taheri-Garavand

Mechanical Engineering of Biosystems Department,
Lorestan University,
Khorramabad, 68138-33946, Iran
Email: taheri.am@lu.ac.ir

Marcus A. Amuche

Department of Mechanical Engineering,
Federal University of Petroleum Resources,
Effurun, Delta State P.M.B 1221, Nigeria
Email: amuchmacs@yahoo.com

Christopher C. Enweremadu

Department of Mechanical Engineering,
University of South Africa,
Science Campus, Private Bag X6, Florida 1709, South Africa
Email: enwercc@unisa.ac.za

Abstract: The analysis of the effects of variables when selecting automotive parts operating in biodiesel medium is critical. This novel study employs RSM and 5-fold cross-validation of ANN in the optimisation strategy for minimising corrosion rates (CRs) of automotive parts (APs) in a biodiesel environment. The hardness number (BHN) and tensile strength (TES) as well as the surface morphologies of copper and brass were investigated. The optimum CRs were

0.01656 mpy and 0.008189 mpy at a B 3.91 biodiesel/diesel blend and 240.9-hour exposure. The established ANN model configuration proved superior adaptability and nonlinearity. The ANN model had higher R^2 and lower values of RMSE, MAE, and AAD when compared to the RSM model, thus validating the superiority of the ANN model. Brass exhibited greater TES while copper had a higher BHN. The database, model, and correlations can assist in mitigating and effectively planning against the corrosiveness of APs when using biodiesel.

Keywords: RSM; response surface methodology; ANN; artificial neural network; corrosion; copper; brass; modelling; biodiesel.

Reference to this paper should be made as follows: Samuel, O.D., Taheri-Garavand, A., Amuche, M.A. and Enweremadu, C.C., (2023) 'Corrosion estimation of Cu and Br based automotive parts exposed to biodiesel environment: case of RSM and ANN', *Int. J. Computational Materials Science and Surface Engineering*, Vol. 11, Nos. 3/4, pp.187–210.

Biographical notes: Olusegun David Samuel holds MEng and PhD degrees in Mechanical Engineering. He has been a Researcher Fellow (Part Time basis) at University of South Africa (UNISA). He is currently working as an Associate Professor of Mechanical Engineering at Federal University of Petroleum Resources, Effurun (Nigeria). His research interests have been in the area of alternative fuels (biodiesel, hydrogen, biogas, metal and microbial fuel) production, optimisation and engine testing; solar energy, computational fluid dynamics (CFD), heat and mass transfer, energy and thermofluid.

Amin Taheri-Garavand received his MSc (2010) and PhD (2015) in Mechanical Engineering of Biosystems from University of Tehran (Iran). He was a visiting researcher at University of Naples Federico II (Italy) in 2014–2015. He is currently working as an Associate Professor of Mechanical Engineering of Biosystems Department at Lorestan University (Iran). His research interests include computational intelligence, deep learning CNN and machine vision in food and agriculture.

Marcus A. Amuche holds HND in Mechanical Engineering and he is currently undergoing his Post-graduate degree programme under the supervision of Dr. O.D. Samuel. His research interests have been on corrosion of metals in biofuel, modelling, and general mechanical engineering design.

Christopher C. Enweremadu holds MSc and PhD degrees in Mechanical Engineering. He is a Full Professor in the Department of Mechanical Engineering, University of South Africa. His research interests have been in the area of alternative fuels (biodiesel, bioethanol and biogas) production, optimisation and engine testing; solar energy and energy storage, and heat transfer.

1 Introduction

Given the depletion of fossil resources and the looming threat of an energy crisis, it is essential to develop emerging solutions to address both current and future energy challenges (Rocabruno-Valdés et al., 2019; Elumalai et al., 2018, 2021). Due to its low

environmental impact, biodegradability, and ability to combat global warming, biodiesel is an excellent diesel fuel alternative (Samuel and Gulum, 2019). Transesterification is used to develop biodiesel, which is a cleaner alternative to diesel fuel (Samuel et al., 2022a, 2022b). Factors influencing ester yield include the amount and type of catalyst used, the molar ratio, the temperature, and the time mandatory to produce the ester (Razzaq et al., 2020). Owing to its higher cetane number, greater lubricity, lower sulphur content, and higher flash point, biodiesel has outshone conventional fossil fuels in popularity. It has undesired poor cold flow properties, advanced viscosity, and volatility, and is more disposed to to corrosion or degradation of APs. The corrosive nature of automotive parts is caused by a lack of compatibility with other APs (Estevez et al., 2022). The incompatibility is attributed to numerous features such as hygroscopic flora of biodiesel and biodiesel oxidation temperature, water content, and microbial advance (Samuel and Gulum, 2019; Jakeria et al., 2014). When an engine component comes into contact with fuel, it can cause corrosion, causing the fuel to deteriorate and deviate even further from its specifications (Singh et al., 2012; Thangavelu et al., 2016; Haseeb et al., 2011). For example, in vehicles powered by biodiesel, the use of gaskets, washers, and bushings made from copper as well as brass radiator tubes, cores, and tanks, have been restricted. Recent findings on the corrosion of automotive parts uncovered to biodiesels derived from sunflower oil, palm oil, Pongamia pinnata oil, Jatropha oil, and Schinzochytrium sp. microalgae have been published (Samuel and Gulum, 2019; Fazal et al., 2012; Parameswaran and Krishnamurthy, 2013; Akhabue et al., 2014; Oni et al., 2022).

It is critical for accurate forecasting and monitoring of engine-part durability to have a reliable prediction of the corrosive characteristics of automotive parts exposed to the biodiesel domain. Rocabruno-Valdés et al. (2019) successfully used the ANN model to forecast the corrosion rates (CRs) of automotive parts and reported that the model is suitable for CR estimation. It is repeatedly indispensable to forecast the effectiveness of an exact substance in a given situation as part of assessing the intrinsic corrosiveness of the structure (Rocabruno-Valdés et al., 2019). These computational tools, according to Samuel and Okwu (2019), enable the correlation of non-linear information by establishing a link amid the inputs and outcomes of the system, even if the underlying mathematical principles of the process are unknown. These computational tools can connect the system's input and output variables even when the mathematical fundamentals of the process are unknown. RSM coupled with ANN is one of the tools that is substantially considered. The hybrid RSM-ANN models (HRAMs) are favoured because they are capable of plotting non-linear and multifaceted data in a suitable and resilient manner. RSM in conjunction with ANN is one of the tools that is extensively considered. The HRAMs make it easy to plot and map non-linear and complex data (Samuel et al., 2021). Particle swarm optimisation and anti-bee colony optimisation, for example, are more difficult to use and require more training to master than the HRAMs (Samuel et al., 2022). The ability of ANN model to correlate non-linear and complex data is what makes it so robust. The lack of a black-box learning mechanism, on the other hand, is largely responsible for ANN's inability to correlate response and dependent parameters (Gupta and Sharma, 2014). The RSM is combined

with other approaches to link responses and corrosion variables to resolve the shortcoming in the ANN model and generate a reliable corrosion prediction.

Table 1 summarises the concise review of the various model tools used to predict metal corrosion rates. Although numerous attempts have been made to model and forecast CRs of various metals in various media using various model tools, only Rocabruno-Valdés et al. (2019) have used ANN models to predict CRs of copper, aluminium, cast iron, mild steel, and mild steel in methyl esters of canola, soybean, chicken, and pork (CSCP). As far as the authors are aware, there is no prior research on the combination of RSM and ANN-based modelling of CRs of waste frying oil biodiesel (WFOB). In order to stop the scarcity in the literature and reduce the corrosiveness of APs in biodiesel, (i) the simultaneous impact of fuel types (0%, 10%, and 10%) and exposure duration (240, 480, and 720 hours) on the CRs of copper and brass of RSM, (ii) the synergic effects of corrosion variables were scrutinised, and (iii) a study on the interaction effects between corrosion variables was investigated.

The evaluations of the hybrid models will demonstrate the performance of these fuels, their corrosivity, and stability in a fuel-metal system, permitting the definition of the operating conditions required for the viable use of copper and brass in the automotive industry.

Table 1 Review of model tools for corrosion of metals in various media

Metals	*Corrosion media*	*Model tools*	*Remarks*	*References*
Copper, brass, aluminium, Cast iron, mild steel, 304 stainless steel	Methyl esters of (CSCP)	Artificial neural network (ANN)	Efficacy of ANN model authenticated for estimating corrosion rate for oils from CSCP	Rocabruno-Valdés et al. (2019)
Ni-Cr-Mo-V	Simulated deep sea environments	DoE and ANN	DoE model exhibited good validity and precision	Hu et al. (2019)
Magnesium alloys	0.1 M NaCl solution at room temperature	ANN	Precision prediction of CR within the tested range of compositions	Xia et al. (2016)
Copper	Acid extract of Gnetum Africana (GA)	Factorial DoE (FDoE)	Established suitability of FDoE for optimum GA for reducing corrosion	Nkuzinna et al. (2014)

2 Experimental methodology

2.1 Experimental procedure

WFOB-diesel blends of 10% (B10), 20% (B20), and pure diesel were prepared using the splash method. For 7 minutes, a magnetic stirrer was used to ensure that the blends were thoroughly mixed, and no heating was used. Figure 1 portrays a photograph of the various types of fuels. An ASTM standard regulatory assessment was performed on the fuel types.

Figure 1 Fuel types prepared for corrosion analysis (see online version for colours)

Experiment coupons were machined from brass and copper bars. The chemical composition and dimensions of the coupons are depicted in Figure 2(a) and (b). To prevent atmospheric corrosion, the coupons were degreased, polished, soaked in acetone for 30 min, weighed, and then stored in desiccators. The prepared coupons were then submitted to static immersion, as described by Aquino et al. (2012) (See Figure 3(a) and (b)). Aquino et al. (2012) investigated the CRs of brass and copper at a temperature of 55°C. The approach used is compliant with ASTM G1 and ASTM G31 regulations (Standard, 2011). Computation of the CRs of copper and brass in response to various fuel sources were made using equations (1) and (2). Pre-exposure and post-exposure measurements of thermophysical fuel types were analysed. Details of the accuracy of equipment utilised are discussed elsewhere (Samuel and Gulum, 2019).

$$CR_{Cu} = \frac{W_{Cu} \times 534}{D_{Cu} A_{Cu} T_{Cu}} \tag{1}$$

$$CR_{Br} = \frac{W_{Br} \times 534}{D_{Br} A_{Br} T_{Br}} \tag{2}$$

where CR_{Cu}, CR_{Br} are the CRs of the copper and brass, W_{Cu}, W_{Br} are the weight losses in copper and copper (mg): the difference between weight prior to immersion and weight after immersion, D_{Cu}, D_{Br} are the densities of copper and brass (g/cm^3), and T_{Cu}, T_{Br} is the exposure duration of copper and brass to WFOB (hours), respectively.

Figure 2 Specification for Br and Cu: (a) dimension (b) chemical composition (see online version for colours)

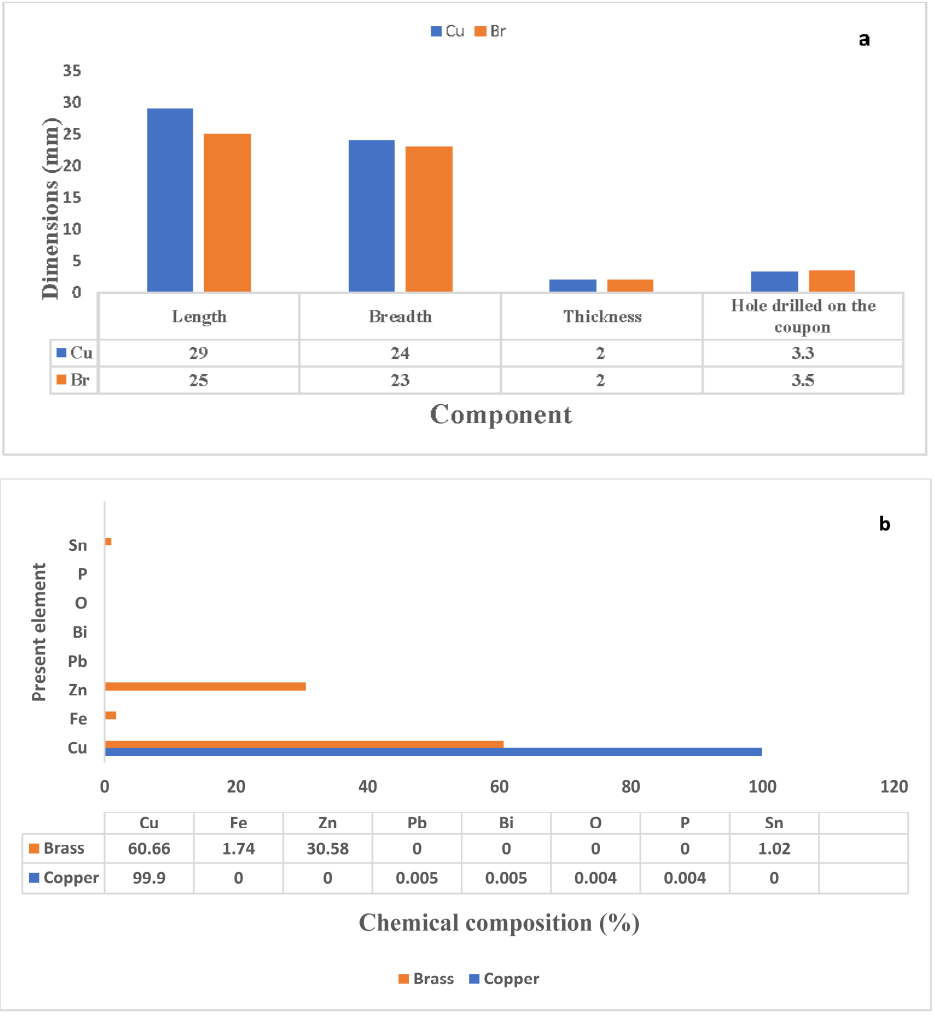

	Length	Breadth	Thickness	Hole drilled on the coupon
Cu	29	24	2	3.3
Br	25	23	2	3.5

	Cu	Fe	Zn	Pb	Bi	O	P	Sn
Brass	60.66	1.74	30.58	0	0	0	0	1.02
Copper	99.9	0	0	0.005	0.005	0.004	0.004	0

Figure 3 Schematic for immersion of corrosion testing of coupons: (a) Cu and (b) Br (see online version for colours)

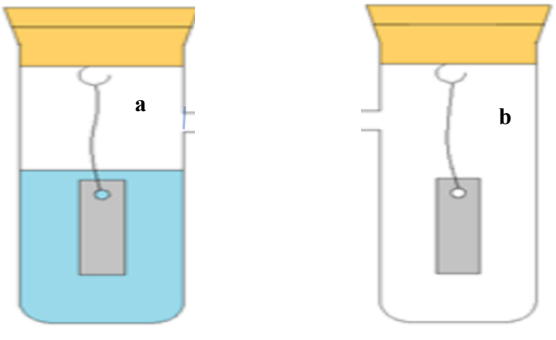

2.2 Uncertainty analysis of corrosiveness of automotive parts

There is a range of operational and static immersion tests on fuel, as well as corrosion studies of automotive features, which results in some ambiguity. For the time being, an uncertainty examination of the precision of the experimentation in conjunction with repeatability is required for certifying the accuracy of the experimental setup.

Table 2 summarises the uncertainty of all measurements. As discovered, the valuation of critical parameters is presented. The measuring equipment's uncertainty analysis was carried out using the standard technique described elsewhere (Holman, 2012). The experiment's overall uncertainty analysis was determined using equation (3). Table 2 summarises the uncertainty of all measurements.

$$\begin{aligned}\text{Overall uncertainity} = \text{square root of}\{&(\text{uncertainity of exposure duration of Cu / Br})^2 \\ &+ (\text{uncertainity of weight loss by Cu})^2 + (\text{uncerainity of weight loss by Br})^2\}\end{aligned} \tag{3}$$

$$\begin{aligned}\text{Overall uncertainity} &= \text{square root of}\left\{(0.707107)^2 + (0.003514)^2 + (1.93431)^2\right\} \\ &= \text{Overall uncertainty} = 1.63\ \%;\ \text{i.e. within the range}\end{aligned}$$

Table 2 Uncertainty assessment of corrosion test of automotive parts

S. No.	*Measuring instruments*	*Uncertainty*
1	Uncertainity of exposure duration of Cu/Br	0.7071
2	Uncertainity of weight loss by Cu	0.003514
3	Uncerainity of weight loss by Br	1.93431

2.3 Measurement of BHN and TES of degraded Cu and Br

The Brinell hardness number (BHN) of degraded Cu and Br exposed to various fuel types under optimal conditions was determined using ASTM standard E10-17. The percent BHN was calculated by averaging the results of three consecutive runs of experiments using equation (4).

$$\%\Delta BHN = 100 \times \left| \frac{BHN_{AE2} - BHN_{BE1}}{BHN_{BE1}} \right| \tag{4}$$

Corroded coupons were tested for tensile strength (TES, MPa) and percent variation using equations (5) and (6), respectively.

$$TES = \frac{34}{10} BHN \tag{5}$$

$$\%\Delta TES = 100 \times \left| \frac{TES_{AE2} - TES_{BE1}}{TES_{BE1}} \right| \tag{6}$$

The morphology of the coupons (brass and copper) immersed in the fuel types was inspected using a JCM 100 small scanning electron microscope (Joel, USA).

2.4 Model techniques

2.4.1 Corrosion study via RSM

This experiment used the Central Composite Design (CCD) component of the response surface methodology (RSM). The CRs of copper and brass exposed to different fuel types can be analysed by examining the linear, quadratic, and interaction impacts of corrosion factors. Table 3 displays the face-centered CCD that was accomplished using Design Expert, which uses a three-level, two-factor CCD for the variables. This section involves the choice of optimum corrosion conditions for minimising the corrosivity of fuel types susceptible to Br and Cu. The RSM was used to perform independent variable optimisation. The development of the RSM model takes into account not only the responses (CR_{Cu} and CR_{Br}), but also a number of independent variables (fuel kinds and exposure length). The CCD approach was used to evaluate the impact of fuel types and exposure duration on the CRs of Cu and Br in this investigation. Figure 4 depicts the steps involved in corrosion modelling using the RSM technique. Two sets of data are used to generate an output: fuel type (B0–B20)/(WFOB0-WFO20) and exposure time (240–720 h) (See Table 3).

Table 3 Variable and levels for RSM based corrosion analysis for Cu and Br

Variables	*Levels*	
	Lower	*Upper*
Biodiesel blends (%) (X_1)	0	20
Exposure duration (hours) (X_2)	240	720

Figure 4 RSM protocol for corrosion (see online version for colours)

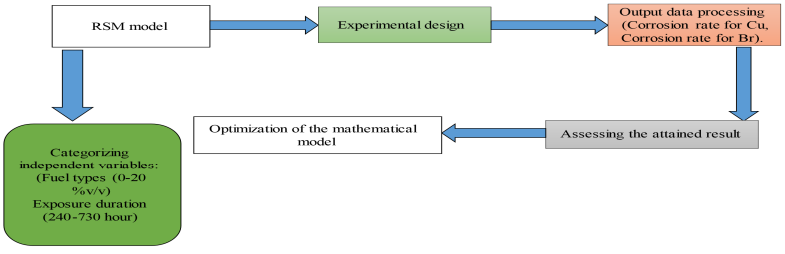

2.4.2 Corrosion modelling via ANN

MATLAB 7.10 R2015a was utilised in the creation of the ANN model (The Neural Network Toolbox, Inc., USA). The ANN model used in this research was a feed-forward structure with three layers: an input layer, a hidden layer, and an output layer. Three neurons were used in the input layer and one neuron was used in the output layer for both Cu and Br CRs. Table 4 highlights the neural network model's details. The RSM design's CCD datasets were fed into the ANN model; these datasets each indicated a different set of CRs for automotive processes and corrosion factors (fuel type and exposure duration).The schematic representation of the ANN model and 5-fold cross-validation employed to predict the CRs of Cu and Br are depicted in Figure 5. The mean square error (MSE) and correlation coefficient (R) are used as the two most popular

statistical indices which are used to assess the recital and accurateness of the network. Models are typically chosen based on their ability to produce the lowest possible mean square error and the highest possible correlation coefficient. Reports indicate that R-values more than 0.9 indicate excellent model efficiency, R-values between 0.8 and 0.9 indicate satisfactory model performance, and R-values less than 0.8 indicate inadequate model performance (Ahmadi et al., 2013). Statistical measures like the correlation coefficient (R), the regression coefficient (R^2), the root mean square error (RMSE), the mean average error (MAE), the standard error of prediction (SEP), and the absolute standard deviation (ASD) were employed to assess the efficacy of the model techniques and their ability to predict outcomes (AAD). Statistics for both the RSM and ANN models were calculated using equations (7)–(12). Success and prominence of the model procedures were evaluated by the results.

$$R = \left(\frac{\sum_{m=1}^{n} (Z_{pre,m} - Z_{pred})(Z_{exp.m} - Z_{exp})}{\sqrt{\sum_{m=1}^{n} (Z_{pre.m} - Z_{pred})^2 \sum_{m=1}^{n} (Z_{exp.m} - Z_{exp})^2}} \right) \tag{7}$$

$$R^2 = 1 - \frac{\sum_{i=1}^{n} (Z_{i,p} - Z_{1,e})^2}{\sum_{i=1}^{n} (Z_{i,p} - Z_{e,ave})^2} \tag{8}$$

$$MSE = \sqrt{\frac{\sum_{i=1}^{n} (Z_{i,e} - Z_{i,p})^2}{n}} \tag{9}$$

$$MAE = \sum_{i=1}^{n} \frac{\left\lfloor (Z_{i,e} - Z_{i,p}) \right\rfloor}{n} \tag{10}$$

$$SEP = \frac{RMSE}{Y_{e,ave}} \tag{11}$$

$$AD = \frac{100}{n} \sum_{i=1}^{n} \frac{\left\lfloor (Z_{i,e} - Z_{i,p}) \right\rfloor}{(Z_{i,e})} \tag{12}$$

Table 4 Particulars for the neural network model

Parameters	*ANN*
Number of input layer units	2
Number of hidden layer	1
Number of hidden layer units	3–10
Number of output layer units	1
Transfer function in hidden layer	Tansig
Transfer function in hidden layer	Purelin
Training function	Levenberg-Marquardt
Learning rate	0.01
Performance goal	0
Maximum number of epoch	100

Figure 5 Flow chart of ANN model with 5-fold cross validation (see online version for colours)

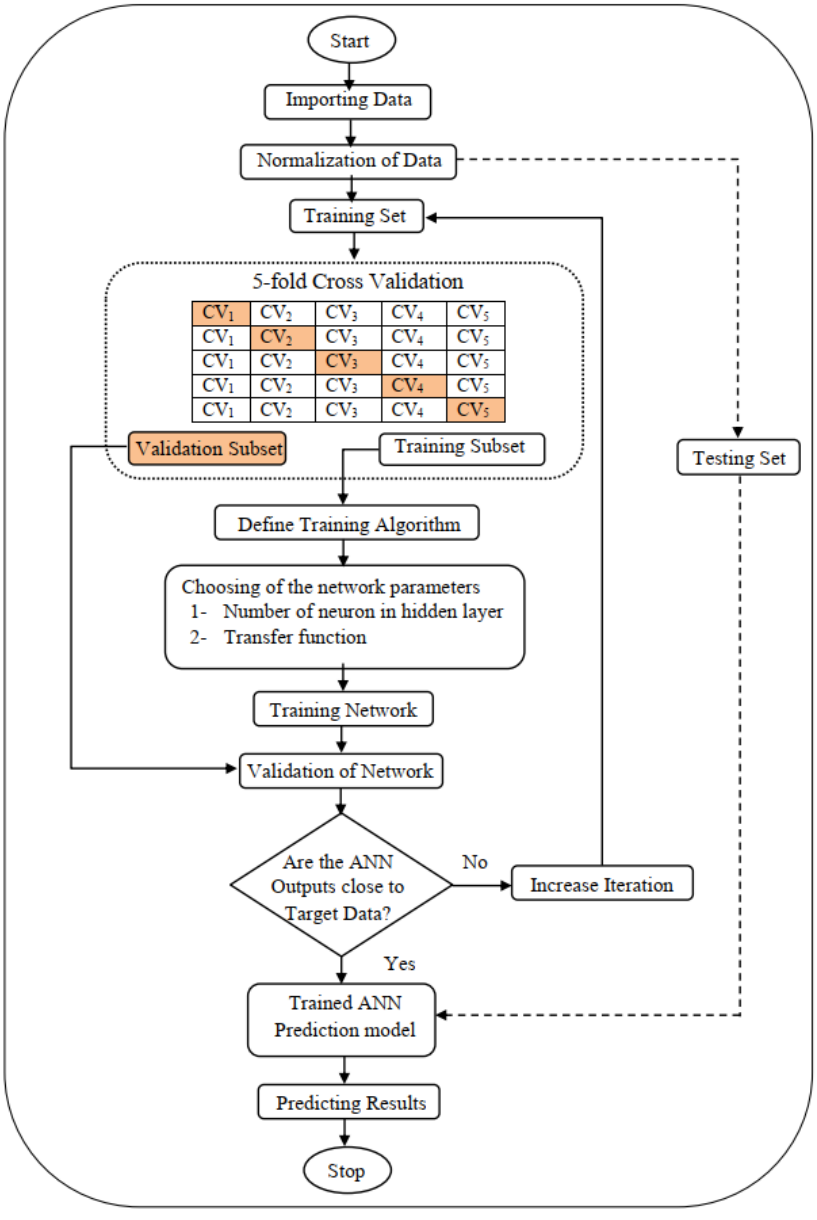

3 Results and discussion

3.1 WFOB's fatty acid composition and fuel physicochemical qualities

The fatty acid content is shown in Figure 6. 84.6% of WFOB's total weight is saturated, while the remaining 15.4% is unsaturated. Samuel et al. (2022) hinted that saturated acid in WFOB can increase NOx while enhancing cetane number at the same time.

Figure 6 Fatty acid composition of WFOB (see online version for colours)

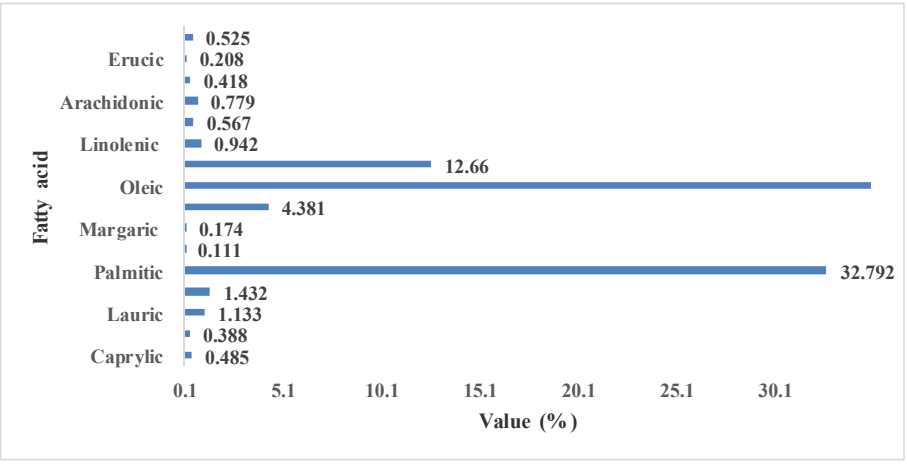

The biodiesel produced must meet the EN 14214 specification's certification requirements in order to be considered commercially viable. Table 5 lists the characteristics of the various fuels. The major properties were found to meet European standards. Since the fuel types have not changed significantly, the diesel engine does not need to be adjusted (Samuel et al., 2019).

Table 5 Properties of fuel for corrosion study

	Types of fuel				
Fuel properties	*B0*	*B10/WFOB10*	*B20/WFOB20*	*B100/WFOB100*	*EN 41214*
Density (kg/m^2)	861.3	862.6	865.3	883.6	850–900
Viscosity (mm^2/s) @ 40°C	4.7162	4.7614	4.8910	5.1282	3.5–5.0
Flash point (°C)	72	74	78	142	120 min
Acid value (mg KOH/g)	0.12	0.14	0.17	0.298	0.50 max

3.2 Modelling and prognostic competence of RSM and analysis of variance (ANOVA) for corrosion rate

Table 6 presents the design layout for the corrosion examination of copper and brass in WFOB. As observed, the highest CRs of copper (0.2429 mpy) and brass (0.1840 mpy) were achieved at a blend ratio of 20% and exposure duration of 720 h while the minimum CRs of copper (0.0173 mpy) and brass (0.0110 mpy) were achieved at a blend ratio of unblended diesel (B0) and exposure duration of 240 h.

Table 7(a) and (b) highlight the ANOVA for the CRs of Cu and Br bare to WFOB, respectively. As observed in Table 7(a), the model F-value of 264.28 infers the model is substantial. This great value of an F-value cannot be explained by random chance alone; the probability is only 0.01%. When the probability of a term in the model is smaller than 0.0500, we say that it is significant. In this case, the quadratic terms of fuel type (A^2) and

exposure duration (B^2) are as important as the linear terms of fuel type (A). However, other factors are not significant. For instance, if the number is higher than 0.1000, it means that the model terms are not important. Model reduction can be useful if your model has a large number of irrelevant terms (excluding those necessary to maintain hierarchy). The model F-value of 12.23, as shown in Table 7(b), also indicates the model's significance. It's not as close as one may assume between the 'Pred R-Squared' value of 0.4266 and the 'Adj R-Squared' value of 0.6709. Possible issues with your model and/or data may be indicated by this. Model simplification, data translation, the identification of outliers, etc. The 'Adeq Precision' metric evaluates the quality of the signal over the background noise. We favour ratios higher than 4. A signal strength of 9.554 shows sufficient ratio. Using this model, you may further explore potential layout options.

Table 6 Design matrix for the corrosion of copper and brass

Coded process variables		*Experimental data*		*Predicted data by RSM*	
Blends (v/v%)	*Exposure duration* (hours)	*Corrosion rates of Cu* (mpy)	*Corrosion rates of Br* (mpy)	*Corrosion rates of Cu* (mpy)	*Corrosion rates of Br* (mpy)
0	240	0.0173	0.011	0.0204	0.006
20	240	0.0254	0.0215	0.0238	0.017
0	720	0.1196	0.106	0.1113	0.124
20	720	0.2429	0.184	0.2299	0.136
0	480	0.0753	0.0639	0.0659	0.065
20	480	0.1268	0.0102	0.1268	0.077
10	240	0.017	0.0109	0.0221	0.012
10	720	0.1427	0.109	0.1706	0.13
10	480	0.0971	0.0807	0.0963	0.071
10	480	0.0971	0.0807	0.0963	0.071
10	480	0.0971	0.0807	0.0963	0.071
10	480	0.0971	0.0807	0.0963	0.071
10	480	0.0971	0.0807	0.0963	0.071

The response surface model obtained to estimate the corrosion rate of Cu in WFOB including all experimental variables is represented by equation (13a) in terms of coded experimental variables and equation (13b) in terms of actual experimental variables. Equation (14a) represents the response surface model obtained to estimate the corrosion rate of brass in WFOB in terms of coded experimental variables, while equation (14b) represents the model in terms of real experimental data.

$$CR_{Cu} = 0.096 + 0.030A + 0.074B + 0.029AB \tag{13a}$$

$$\begin{aligned} \mathrm{CR_{Cu}} = {} & -0.025037 - 0.002712 * \text{Blend} + 0.0001894 * \text{Exposure duration} + 0.012 \\ & + 0.029 * \text{Fuel blend} * \text{Exposure duration} \end{aligned} \tag{13b}$$

$$CR_{Br} = 0.071 + 0.0058A + 0.0B + 0.059AB \quad (14a)$$

$$CR_{Br} = -0.053564 + 0.00058 * \text{Blend} + 0.000247 * \text{Exposure duration} \quad (14b)$$

Table 7(a) ANOVA for modelling of corrosion rate of Cu in WFOB

Source	*Sum of squares*	*Df*	*Mean square*	*F-value*	*p-value*	
Model	0.1257	5	0.0251	264.28	<0.0001	*SIG
A-Blend	0.011	1	0.011	115.35	<0.0001	SIG
B-Exposure duration	0.1054	1	0.1054	1108.16	<0.0001	SIG
AB	0.0036	1	0.0036	37.34	0.0005	SIG
A^2	0.0007	1	0.0007	7.03	0.0329	**NSIG
B^2	0.0057	1	0.0057	60.45	0.0001	SIG
Residual	0.0007	7	0.0001			
Lack of fit	0.0007	3	0.0002			
Pure error	0	4	0			
Cor Total	0.1263	12				

*SIG, **NSIG.

Table 7(b) ANOVA for modelling of corrosion rate of brass in WFOB

Source	*Sum of squares*	*Df*	*Mean square*	*F-value*	*p-value*	
Model	0.0213	2	0.0106	13.23	0.0016	SIG
A-Blend	0.0002	1	0.0002	0.2510	0.6272	NSIG
B-Exposure duration	0.9211	1	0.0211	26.21	0.00025	SIG
Residual	0.0080	10	0.0008			
Lack of fit	0.0080	6	0.0013			
Pure error	0.0000	4	0.0000			
Cor Total	0.0293	12				

3.3 Interactive effects of process variables/Parameters on the CRs

Plotting the model's response surface is the best way to visualise the impact of each variable on the response across the space of experiments (Kusuma and Mahfud, 2016). The contour plots (2-dimensional) and the response surfaces (3-dimensional) generated by the model are shown in Figure 7(a)–(d) for all experimental parameters.

As observed in Figure 7(a)–(b), the CR of copper augmented with the upsurge in WFOB fraction and exposure duration. The CR ranged from 0.05 to 0.10 mpy with 10% WFOB and 480 h of exposure duration. The CR became exceedingly aggravated at a higher WFOB and exposure duration. Similar observation was detected by Fazal et al. (2010) and Cursaru et al. (2014). This phenomenon is due to long exposure duration and high biodiesel content, which is attributed to hydrolysis, leading to a high corrosion rate (Zuleta et al., 2012; Gulzar et al., 2016).

Figure 7 Contour and response surface plots for CRs: (a) 2D for CRs of Cu, (b) 3D for CRs of Cu, (c) 2D for CRs of Br, and (d) 3D for CRs of Br (see online version for colours)

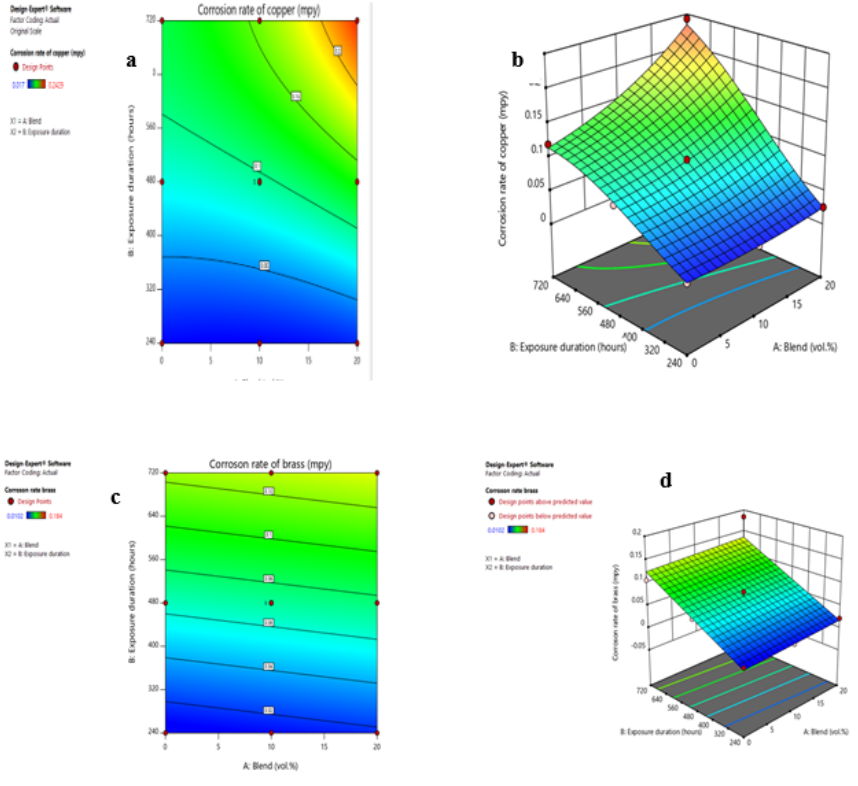

As observed in Figure 8(c)–(d), the CR of brass increased with the increase in WFOB and exposure duration. The CR ranged from 0.05 to 0.10 mpy with 10% WFOB and 480 h of exposure duration. The CR became exceedingly aggravated at a higher WFOB and exposure duration (Chandran et al., 2016).

Figure 8(a) The topology of artificial neural network (see online version for colours)

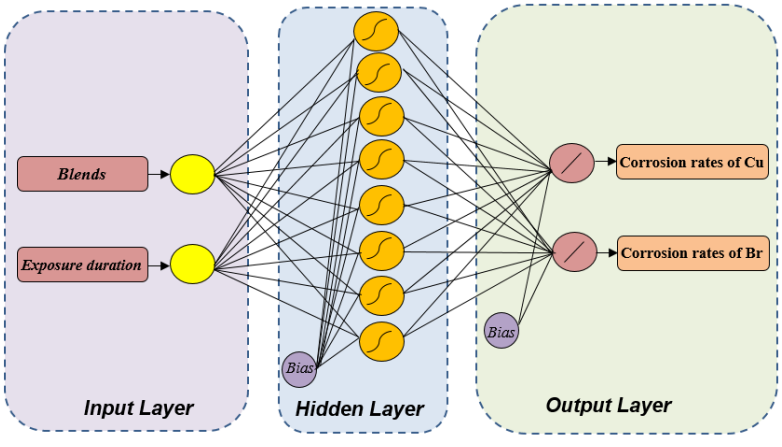

Figure 8(b) Performance-plot of the chosen network (see online version for colours)

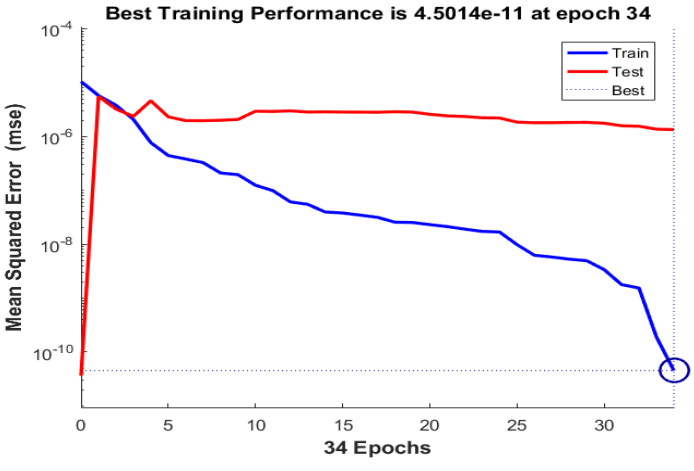

Figure 8(c) Performance of the suitable ANN for the training, testing and validation datasets (see online version for colours)

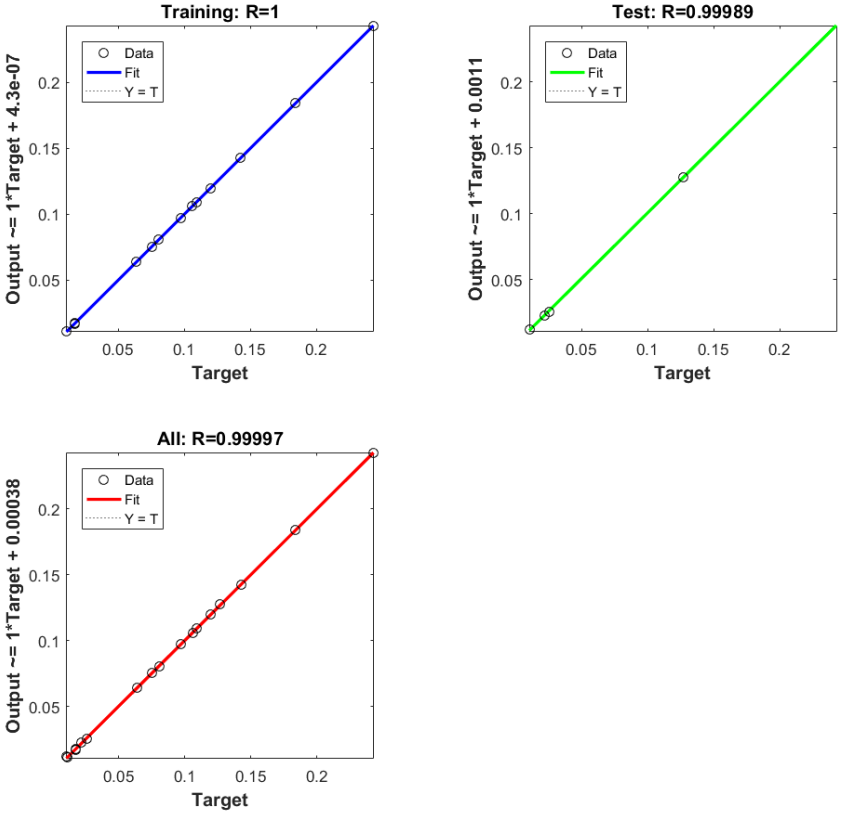

3.4 ANN model for corrosion rates

The ANN architecture is the foundation for perfect prediction (Ranasinghe et al., 2017). Figure 8(a) depicts the schematic of a multilayer ANN. As seen, the input layer consists of two process parameters (fuel blend and exposure length), eight hidden levels, and two layers in the output (corrosion rate of Cu and corrosion rate of Br). Through iterative testing, the optimal condition can be identified. Neurons for the input layer are selected according to the layer that is specified.

The best validation results from a different time period are shown in Figure 8(b). As can be shown, the greatest validation performance is 4.50×10^{-11} at epoch 34, and the lowest MSE value and good prediction of the outputs of both training and test sets were gained with 8 neurons in the hidden layer.

Figure 8(c) shows the output vs. target chart, as well as the observed and predicted outputs for each sample when running for the training, testing, and validation datasets. Training and testing results show the correlation coefficients (R) values of 0.99989 and 0.99997, with 1.0 being a perfect correlation between actual and projected values (validation). This implies that the linear fit regression between the experimental CRs for Br and Cu and the ANN predicted values is ideal.

3.5 Comparing of RSM and ANN models

Figure 9(a) depicts the actual CRs for Cu and Br, as well as those of the HRAMs. As demonstrated, the CRs model from the ANN is very close to the experimental CRs when compared to the model obtained from the RSM for each run. Other researchers have reported similar findings (Samuel et al., 2021; Coşkun and Karahan, 2018; Oguntade et al., 2020).

Figure 9(b)–(c) show RSM prediction CRs vs. experimental CRs for Cu and Br, while Figure 9(d)–(e) show ANN prediction CRs vs. experimental CRs for Cu and Br. The linear equations $(1x+0.00001)$ and $(1.0014x-0.0003)$ are discovered to be adequate for the variations of experimental and RSM-based CRs, respectively, whereas the linear equations $(0.9993x+0.00002)$ and $(1.0057x-0.0006)$ are also found to be appropriate for these same variations for copper and brass, respectively. The RSM had an R^2 of 0.7254 and 0.9734 for the CRs of brass and copper, while the ANN had an R^2 of 0.9999 and 1.0, indicating that the ANN model captured a greater proportion of the data than the RSM model. As a result, the ANN model could predict CRs for brass and copper in a biodiesel environment. Comparable reports were expressed by researchers elsewhere (Samuel et al., 2022; Li et al., 2022)

It is critical to compare the superiority of RSM and ANN in predicting the CRs of Cu and Br in a biodiesel environment in order to get accurate predictions. Various statistical criteria were used to compare the RSM and ANN models in this study's prediction power comparison. Bar graphs in Figure 9(f) show statistical index values associated with the comparison of RSM and ANN performance. According to statistical bar graphs, ANN models outperform RSM models.

Figure 9(a) Runs vs. experimental, RSM, and ANN predicted corrosion rates (see online version for colours)

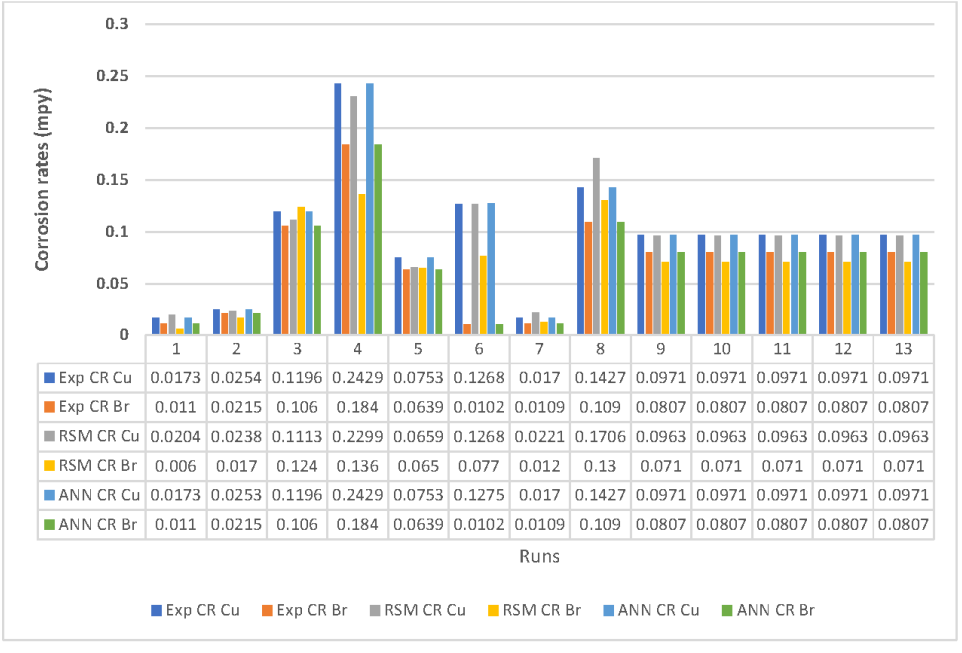

	1	2	3	4	5	6	7	8	9	10	11	12	13
Exp CR Cu	0.0173	0.0254	0.1196	0.2429	0.0753	0.1268	0.017	0.1427	0.0971	0.0971	0.0971	0.0971	0.0971
Exp CR Br	0.011	0.0215	0.106	0.184	0.0639	0.0102	0.0109	0.109	0.0807	0.0807	0.0807	0.0807	0.0807
RSM CR Cu	0.0204	0.0238	0.1113	0.2299	0.0659	0.1268	0.0221	0.1706	0.0963	0.0963	0.0963	0.0963	0.0963
RSM CR Br	0.006	0.017	0.124	0.136	0.065	0.077	0.012	0.13	0.071	0.071	0.071	0.071	0.071
ANN CR Cu	0.0173	0.0253	0.1196	0.2429	0.0753	0.1275	0.017	0.1427	0.0971	0.0971	0.0971	0.0971	0.0971
ANN CR Br	0.011	0.0215	0.106	0.184	0.0639	0.0102	0.0109	0.109	0.0807	0.0807	0.0807	0.0807	0.0807

Figure 9 Contrast of the various corrosion rates: (b) RSM predicted and experimental CRs for Cu; (c) RSM predicted and experimental CRs for Br; (d) ANN predicted and experimental CRs for Cu and (e) ANN predicted and experimental CRs for Br (see online version for colours)

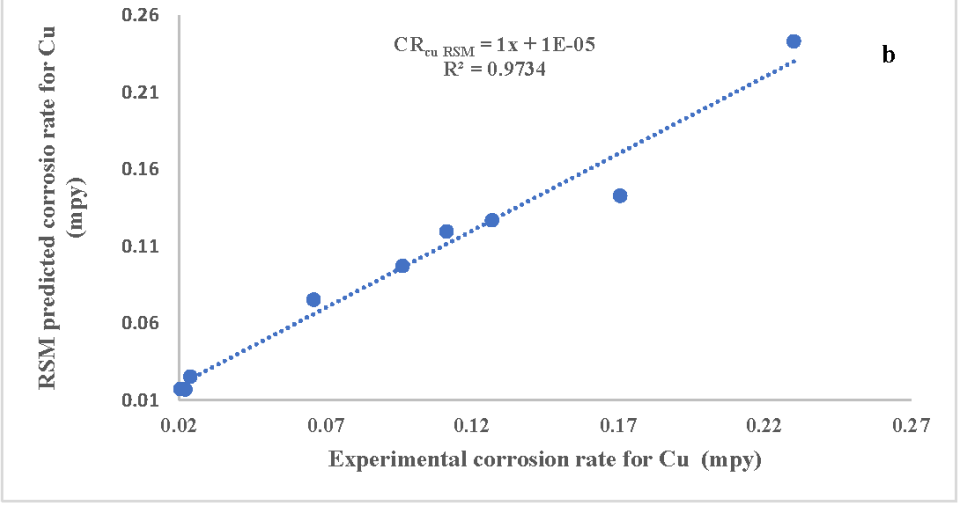

Figure 9 Contrast of the various corrosion rates: (b) RSM predicted and experimental CRs for Cu; (c) RSM predicted and experimental CRs for Br; (d) ANN predicted and experimental CRs for Cu and (e) ANN predicted and experimental CRs for Br (see online version for colours) (continued)

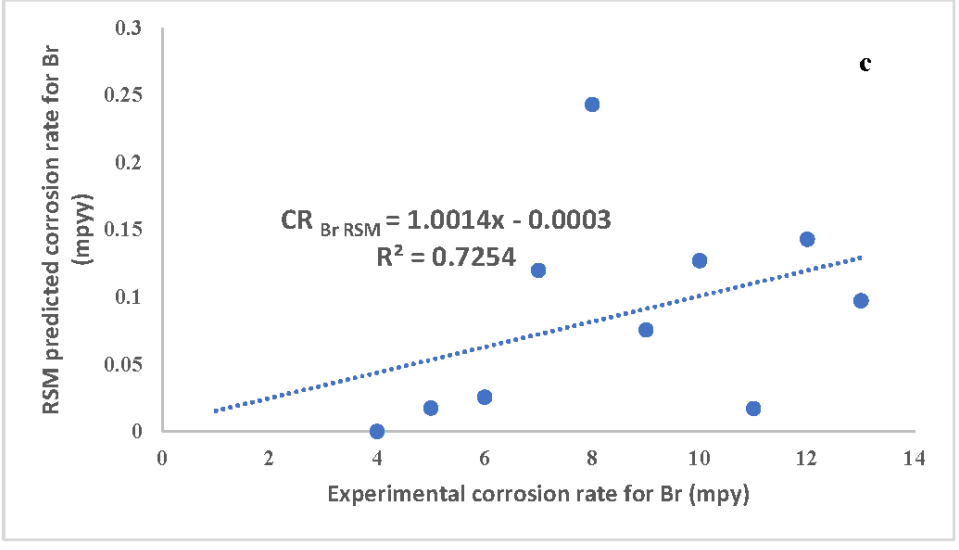

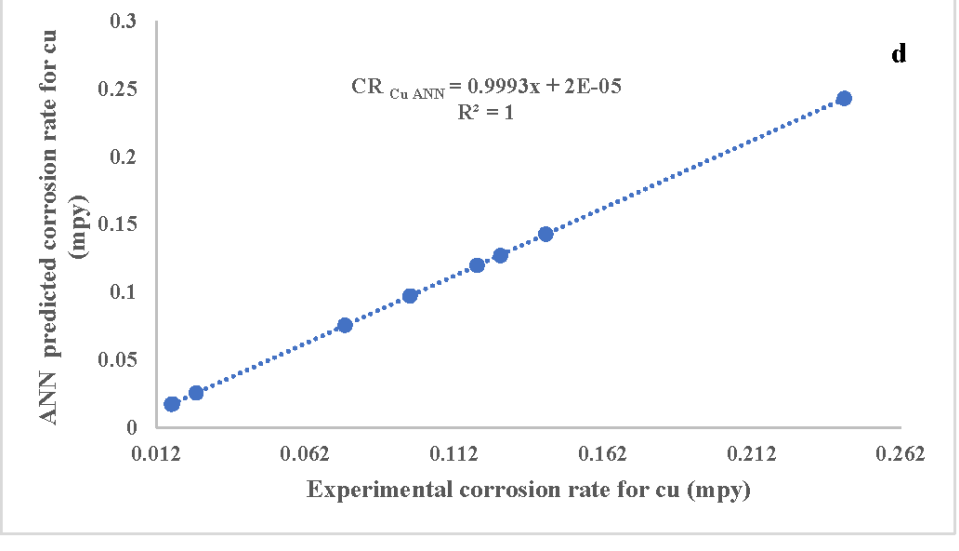

Figure 9 Contrast of the various corrosion rates: (b) RSM predicted and experimental CRs for Cu; (c) RSM predicted and experimental CRs for Br; (d) ANN predicted and experimental CRs for Cu and (e) ANN predicted and experimental CRs for Br (see online version for colours) (continued)

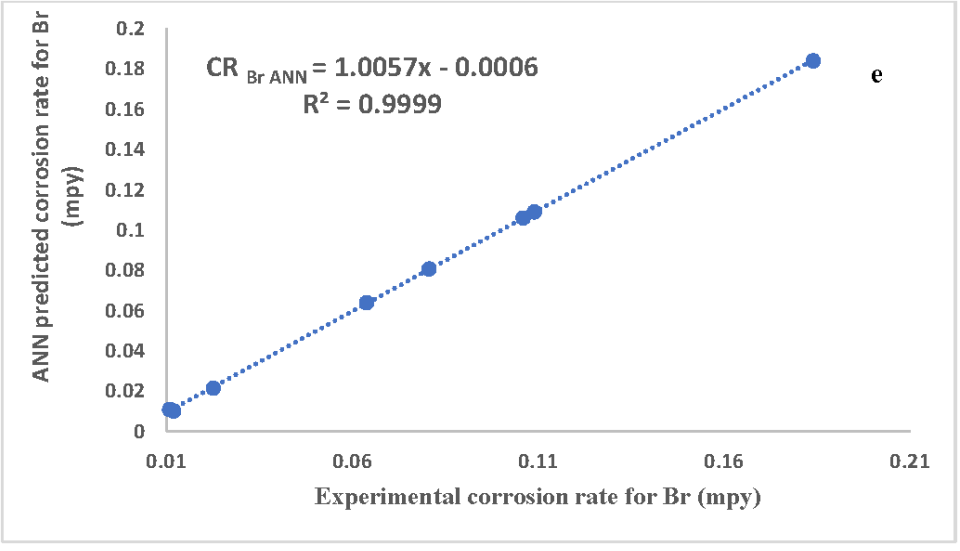

Figure 9(f) Catalogues of RSM and ANN models (see online version for colours)

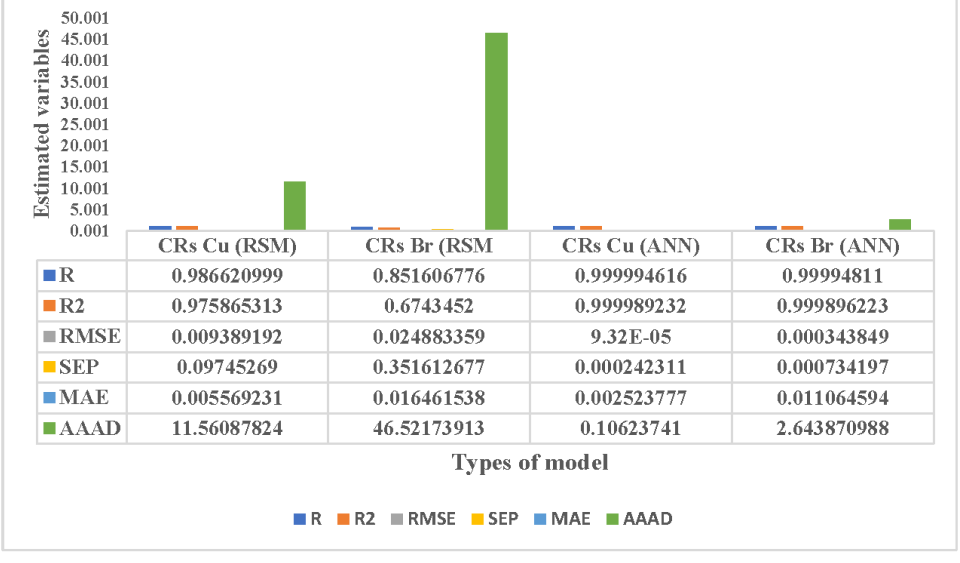

	CRs Cu (RSM)	CRs Br (RSM	CRs Cu (ANN)	CRs Br (ANN)
R	0.986620999	0.851606776	0.999994616	0.99994811
R2	0.975865313	0.6743452	0.999989232	0.999896223
RMSE	0.009389192	0.024883359	9.32E-05	0.000343849
SEP	0.09745269	0.351612677	0.000242311	0.000734197
MAE	0.005569231	0.016461538	0.002523777	0.011064594
AAAD	11.56087824	46.52173913	0.10623741	2.643870988

3.6 Corrosions' optimal condition for minimisation and its mechanical properties

Figure 10(a) depicts the optimal conditions for minimising Cu and Br CRs in a biodiesel environment. The CRs of Cu (0.01656 mpy) and Br (0.008189) were found to be optimal at B 3.91 of biodiesel/diesel blend and exposure duration of 240.9 h. Optimised

experimental variables led to experimental CRs of 0.01655 mpy and 0.0081865 mpy for Cu and Br, respectively, in a justification test. Comparing forecasted and measured CRs for Cu and Br, the average error was 0.06% and 0.03054%, respectively. Good agreement between the percentages of error in prediction was found during validation, proving that the RSM model developed was reliable. Table 8 shows the mechanical properties of Cu and Br exposed to biodiesel at optimal conditions, namely BHN and TES. As can be seen, the TES of Br was higher than copper while the hardness of the latter exceeded that of the former. According to Chandran et al. (2016), the higher hardness number and tensile strength are due to higher oxygen dissociation and better conductivity of optimal corroded biodiesel of Br to Cu.

Figure 10(a) Optimal condition for corrosion minimisation for Cu and Br in biodiesel environment (see online version for colours)

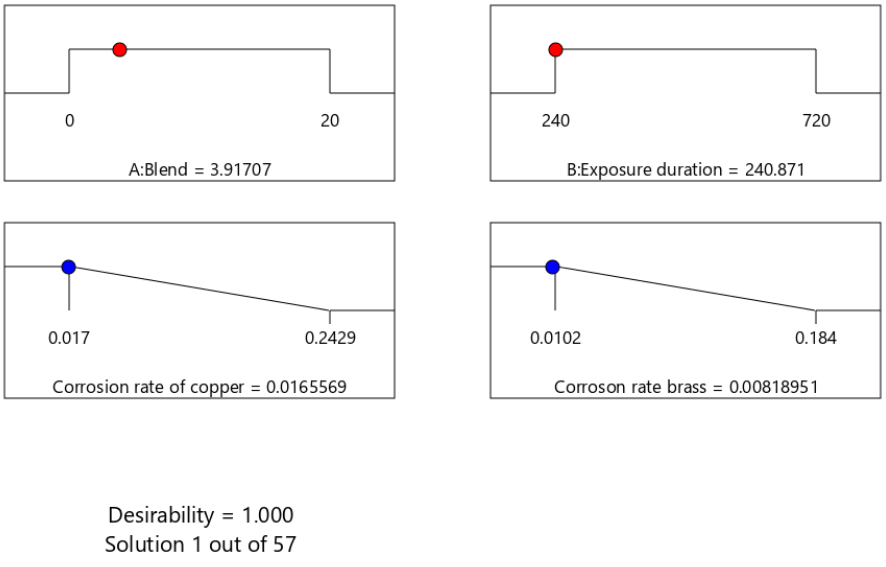

Table 8 Mechanical properties of corroded Cu and Br

AP[*]	*Hardness number* (N/mm^2)	*Tensile strength* (MPa)
Cu	211.12	717.80
Br	68.63	1476.52

[*]Automotive parts.

3.7 Surface morphology of the automotive parts

Figure 10(b) depicts the micrograph surface (MS) of copper and brass under optimal conditions. When compared to brass, the MS of copper darkens. This phenomenon can be explained by the greater computability of brass to copper.

Figure 10(b) SEM Morphologies of Cu and Br: (a) Cu before exposure; (b) Cu after exposure; (c) Br before exposure and (d) Br after exposure

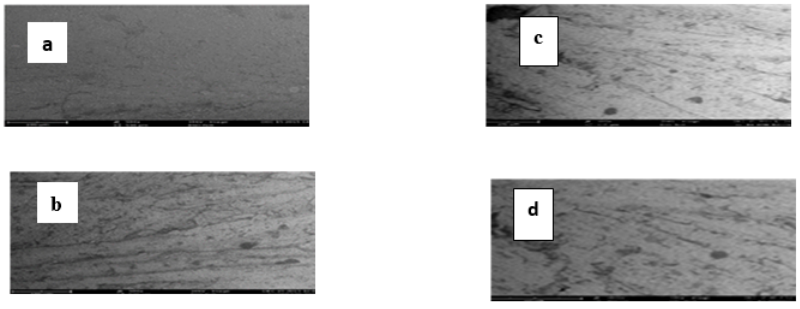

4 Conclusion

The study demonstrated the prediction and modelling of copper and brass CRs in biodiesel synthesised using RSM and ANN models. The best conditions and correlations for predicting and modelling the CRs of these automotive parts were identified. The mechanical properties of automotive parts, specifically BHN and TES, as well as surface morphologies prior to exposure and under optimal conditions, were investigated. To achieve a vigorous study in the close imminent, (i) supplementary operating corrosion variables can be studied, (ii) the inclusion and efficacy of cost-effective inhibitors can be studied, and (iii) kinetic and thermodynamic features can be studied further. The optimum CRs for copper and brass were 0.01656 mpy and 0.008189 mpy at a B 3.91 biodiesel/diesel blend and 240.9-h exposure. The developed ANN model configuration (2-13-2) demonstrated greater adaptability and nonlinearity. When compared to the RSM model, the ANN model had a higher coefficient of determination and lower values of root mean squared errors (RMSE), MAE, and average absolute deviation (AAD); this validates the ANN model's superiority for predicting CRs of copper and brass. The tensile strength of brass was greater than that of copper, while the latter had a higher hardness number.

Acknowledgements

For the use of their JCM 100 small scanning electron microscope, the authors would like to thank the Chemical Engineering Department at Ahmadu Bello University.

References

Ahmadi, M., Ebadi, M., Shokrollahi, A. and Majidi, S. (2013) 'Evolving artificial neural network and imperialist competitive algorithm for prediction oil flow rate of the reservoir', *Applied Soft Computing.*, Vol. 13, No. 2, pp.1085–1098, doi: org/10.1016/j. asoc.2012.10.009.

Akhabue, C., Aisien, F. and Ojo, C. (2014) 'The effect of jatropha oil biodiesel on the corrosion rates of aluminium and mild carbon steel', *Biofuels*, Vol. 5, No. 5, pp.545–550, doi: org/ 10.1080/17597269.2014.1002995.

Aquino, I.P., Hernandez, R.P., Chicoma, D.L., Pinto, H.P. and Aoki, I.V. (2012) 'Influence of light, temperature and metallic ions on biodiesel degradation and corrosiveness to copper and brass', *Fuel*, Vol. 102, pp.795–807, doi: org/10.1016/j. fuel.2012.06.011.

Chandran, D., Ng, H.K., Lau, H.L., Gan, S. and Choo, Y.M. (2016) 'Investigation of the effects of palm biodiesel dissolved oxygen and conductivity on metal corrosion and elastomer degradation under novel immersion method', *Appl. Therm. Eng.*, Vol. 104, pp.294–308, doi: org/10.1016/j. applthermaleng.2016.05.044.

Coşkun, M.İ. and Karahan, İ.H. (2018) 'Modeling corrosion performance of the hydroxyapatite coated coCrMo biomaterial alloys', *Journal of Alloys and Compounds.*, Vol. 745, pp.840–848, doi: org/10.1016/j. jallcom.2018.02.253.

Cursaru, D.L., Brănoiu, G., Ramadan, I. and Miculescu, F. (2014) 'Degradation of automotive materials upon exposure to sunflower biodiesel', *Industrial Crops and Products.*, Vol. 54, pp.149–158, doi: org/10.1016/j. indcrop.2014.01.032.

Elumalai, P., Sivakandhan, C., Parthasarathy, M., Mohamed Iqbal, S. and Arunkumar, M. (2021) 'Investigation on the mitigation of environmental harmful emissions by incorporating nanoparticles to biofuel water nano emulsion in low heat rejection engine', *Heat and Mass Transfer.*, Vol. 57, No. 8, pp.1235–1250, https://doi.org/10.1007/s00231-021-03028-7

Elumalai, V.E., Kandhasamy, A., Subramani, L., Sivalingam, A. and Kumar, A. (2018) 'Experimental investigation on lemongrass oil water emulsion in low heat rejection direct ignition diesel engine', *Journal of Testing and Evaluation.*, Vol. 47, No. 1, pp.238–255, doi: 10.1520/JTE20170357.

Estevez, R., Aguado-Deblas, L., López-Tenllado, F., Luna, C., Calero, J., Romero, A.L. and D. (2022) 'Biodiesel is dead: long life to advanced biofuels–a comprehensive critical review', *Energies*, Vol. 15, p.3173, doi: org/10.3390/en15093173.

Fazal, M.A., Haseeb, A.S. and Masjuki, H.H. (2010) 'Comparative corrosive characteristics of petroleum diesel and palm biodiesel for automotive materials', *Fuel Processing Technology.*, Vol. 91, No. 10, pp.1308–1315.

Fazal, M., Haseeb, A. and Masjuki, H. (2012) 'Degradation of automotive materials in palm biodiesel', *Energy*, Vol. 40, No. 1, pp.76–83, doi: org/10.1016/j. energy.2012.02.026.

Gulzar, M., Masjuki, H., Varman, M., Kalam, M., Zulkifli, N., Mufti, R. and Arslan, A. (2016) 'Effects of biodiesel blends on lubricating oil degradation and piston assembly energy losses', *Energy.*, Vol. 111, pp.713–721, doi: org/10.1016/j. energy.2016.05.132.

Gupta, A. and Sharma, D. (2014) 'A survey on stock market prediction using various algorithms', *International Journal Computer Technology and Applications.*, Vol. 5, pp.530–533.

Haseeb, A.S., Fazal, M.A., Jahirul, M.I. and Masjuki, H.H. (2011) 'Compatibility of automotive materials in biodiesel: a review', *Fuel*, Vol. 90, No. 3, pp.922–931.

Holman, J. (2012) *Experimental Methods for Engineers*, McGraw-Hill.

Hu, Q., Liu, Y., Zhang, T., Geng, S. and Wang, F. (2019) 'Modeling the corrosion behavior of ni-Cr-Mo-V high strength steel in the simulated deep sea environments using design of experiment and artificial neural network', *Journal of Materials Science and Technology*, Vol. 35, No. 1, pp.168–175, doi: org/10.1016/j. jmst.2018.06.017.

Jakeria, M., Fazal, M. and Haseeb, A. (2014) 'Influence of different factors on the stability of biodiesel: a review', *Renewable and Sustainable Energy Reviews.*, Vol. 30, pp.154–163, doi: org/10.1016/j. rser.2013.09.024.

Kusuma, H. and Mahfud, M. (2016) 'Response surface methodology for optimization studies of microwave assisted extraction of sandalwood oil', *Journal of Material Environmental Science*, Vol. 7, No. 6, pp.1958–1971.

Li, X., Wang, H., Wang, B. and Guan, Y. (2022) 'Machine learning methods for prediction analyses of 4H–SiC microfabrication via femtosecond laser processing', *Journal of Materials Research and Technology*, Vol. 18, pp.2152–2165, doi: org/10.1016/j. jmrt.2022.03.124.

Nkuzinna, O., Menkiti, M., Onukwuli, O., Mbah, G., Okolo, B. and Egbujor, M. (2014) 'Application of factorial design of experiment for optimization of inhibition effect of acid extract of gnetum Africana on copper corrosion', *Natural Resources,* doi:dx.doi.org/10.4236/nr.2014.57028

Oguntade, T.I., Ita, C.S., Sanmi, O. and Oyekunle, D.T. (2020) 'A binary mixture of sesame and castor oil as an ecofriendly corrosion inhibitor of mild steel in crude oil', *The Open Chemical Engineering Journal.*, Vol. 14, No. 1, pp.25–35, doi: 10.2174/1874123102014010025.

Oni, B., Sanni, S., Ezurike, B. and Okoro, E. (2022) 'Effect of corrosion rates of preheated schinzochytrium sp. microalgae biodiesel on metallic components of a diesel engine', *Alexandria Engineering Journal.*, Vol. 61, No. 10, pp.7509–7528, doi: org/10.1016/j.aej.2022.01.005.

Parameswaran, M.A. and Krishnamurthy, S. (2013) 'A comparison of corrosion behaviour of copper and its alloy in pongamia pinnata oil at different conditions', *Journal of Energy*, pp.1–4.

Ranasinghe, R., Jaksa, M., Kuo, Y. and Nejad, F. (2017) 'Application of artificial neural networks for predicting the impact of rolling dynamic compaction using dynamic cone penetrometer test results', *Journal of Rock Mechanics and Geotechnical Engineering.*, Vol. 9, No. 2, pp.340–349.

Razzaq, L., Imran, S., Anwar, Z., Farooq, M., Abbas, M., Mehmood Khan, H. and Rahman, S. (2020) 'Maximising yield and engine efficiency using optimised waste cooking oil biodiesel', *Energies*, Vol. 13, No. 22, p.5941, doi: org/10.3390/en13225941.

Rocabruno-Valdés, C., González-Rodriguez, J., Díaz-Blanco, Y., Juantorena, A., El-Hamzaoui, Y. and Hernández, J. (2019) 'Corrosion rate prediction for metals in biodiesel using artificial neural networks', *Renewable Energy.*, Vol. 140, pp.592–601, https://doi.org/10.1016/j.renene.2019.03.065

Samuel, O.D., Okwu, M.O., Amosun, S.T., Verma, T.N. and Afolalu, S.A. (2019) 'Production of fatty acid ethyl esters from rubber seed oil in hydrodynamic cavitation reactor: study of reaction parameters and some fuel properties', *Industrial Crops and Products.*, Vol. 141, p.111658, doi: org/10.1016/j. indcrop.2019.111658.

Samuel, O. and Gulum, M. (2019) 'Mechanical and corrosion properties of brass exposed to waste sunflower oil biodiesel-diesel fuel blends', *Chemical Engineering Communications.*, Vol. 206, No. 5, pp.682–694, doi: 10.1080/00986445.2018.1519508.

Samuel, O. and Okwu, M. (2019) 'Comparison of response surface methodology (RSM) and artificial neural network (ANN) in modelling of waste coconut oil ethyl esters production', *Energy Sources, Part A: Recovery, Utilization, and Environmental Effects*, Vol. 41, No. 9, pp.1049–1061, doi: org/10.1080/15567036.2018.1539138.

Samuel, O., Kaveh, M., Oyejide, O., Elumalai, P., Verma, T., Nisar, K., Saleel, C.A., Afzal, A., Fayomi, O.S.I., Owamah, H.I. and Sarıkoç, S. (2022b) 'Performance comparison of empirical model and particle swarm optimization and its boiling point prediction models for waste sunflower oil biodiesel', *Case Studies in Thermal Engineering.*, Vol. 33, p.101947, doi: org/10.1016/j. csite.2022.101947.

Samuel, O., Kaveh, M., Verma, T., Okewale, A., Oyedepo, S., Abam, F., Nwaokocha, C.N., Abbas, M., Enweremadu, C.C., Khalife, E. and Saleel, C. (2022) 'Grey wolf optimizer for enhancing nicotiana tabacum L, oil methyl ester and prediction model for calorific values', *Case Studies in Thermal Engineering*, Vol. 35, 102095, doi: org/10.1016/j. csite.2022.102095.

Samuel, O., Waheed, M., Taheri-Garavand A., Verma, T., Dairo, O., Bolaji, B. and Afzal, A. (2021) 'Prandtl number of optimum biodiesel from food industrial waste oil and diesel fuel blend for diesel engine', *Fuel*, Vol. 285, 119049, doi: org/10.1016/j. fuel.2020.119049.

Singh, B., Korstad, J. and Sharma, Y. (2012) 'A critical review on corrosion of compression ignition (CI) engine parts by biodiesel and biodiesel blends and its inhibition', *Renewable and Sustainable Energy Reviews*, Vol. 16, No. 5, pp.3401–3408, https://doi.org/10.1016/j.rser.2012.02.042

Standard, A.S. (2011) *Standard Practice for Preparing, Cleaning, and Evaluating Corrosion Test Specimens.* American Society for Testing and Materials G1-03.

Thangavelu, S., Ahmed, A. and Ani, F. (2016) 'Impact of metals on corrosive behavior of biodiesel-diesel-ethanol (BDE) alternative fuel', *Renew. Energy*, Vol. 94, pp.1–9, doi: org/10.1016/j. renene.2016.03.015.

Xia, X., Nie, J.F., Davies, C.H., Tang, W.N., Xu, S.W. and Birbilis, N. (2016) 'An artificial neural network for predicting corrosion rate and hardness of magnesium alloys', *Materials and Design.*, Vol. 90, pp.1034–1043, doi: org/10.1016/j. matdes.2015.11.040.

Zuleta, E.C., Rios, L.A. and Calderón, J.A. (2012) 'The oxidative stability of biodiesel and its impact on the deterioration of metallic and polymeric materials: a review', *Journal of the Brazilian Chemical Society.*, Vol. 23, pp.2159–2175, doi: org/10.1590/S0103-5053201200 1200004.